



## Supporting Online Material for

### **Self-Organizing and Stochastic Behaviors During the Regeneration of Hair Stem Cells**

Maksim V. Plikus, Ruth E. Baker, Chih-Chiang Chen, Clyde Fare, Damon de la Cruz, Thomas Andl, Philip K. Maini, Sarah E. Millar, Randall Widelitz, Cheng-Ming Chuong\*

\*To whom correspondence should be addressed. E-mail: [cmchuong@usc.edu](mailto:cmchuong@usc.edu)

Published 29 April 2011, *Science* **332**, 586 (2011)

DOI: 10.1126/science.1201647

#### **This PDF file includes:**

Materials and Methods  
Figs. S1 to S16  
Tables S1 to S3

**Other Supporting Online Material for this manuscript includes the following:**  
available at [www.sciencemag.org/cgi/content/full/332/6029/586/DC1](http://www.sciencemag.org/cgi/content/full/332/6029/586/DC1)

Movies S1 to S9

## Supporting Online Material

### Materials and Methods

**Animals.** C75BL/6J, SCID, *KRT14-NOG* (*K14-Nog*), *KRT14-Wnt7a* (*K14-Wnt7a*), *BAT-gal*, *conductin-lacZ* (*cond-lacZ*), *cond-lacZ;K14-Wnt7a* mice and New Zealand rabbits were studied.

**Analysis of hair regeneration patterns.** Hair regeneration patterns were monitored by periodically clipping fur and photographing the entire animal. Unlike plucking or shaving, the clipping of hair shafts does not affect physiological progression of the hair growth cycle and is non-invasive. Analysis of patterns was done by carefully studying skin pigmentation changes on timelines compiled from many sequential images of the same animal.

**Transplantation procedures.** All surgical procedures were performed on anesthetized animals following a protocol approved by USC animal resources. Skin transplantation was carried out when both donor rabbit and recipient SCID mouse skin were in early telogen. This minimized the impact of wound healing on the hair growth cycle. After transplantation, recipient SCID mice were monitored for a prolonged period of time (~one year). Changes in the hybrid hair regeneration patterns were documented and photographed.

**Protein administration procedures.** Intracutaneous administration of exogenous protein was performed as follows. Affinity chromatography Affi-gel blue gel beads were obtained from Biorad. Beads were washed in 1× PBS, followed by drying. The beads were then re-suspended in 5µl protein solution, either control (0.1% BSA) or experimental (recombinant mouse Wnt3a, 100ug/ml; recombinant mouse Dkk1, 100ug/ml), at 4 °C for 30 min. Both recombinant Wnt3a and Dkk1 were from R&D Systems. Reconstitution of the protein was as per the manufacturer's guidelines. Approximately 100 beads were introduced to the telogen skin of adult mice by means of a single puncture made by a 30G syringe needle. To replenish proteins, subsequent doses of 1.5 µl protein solution were microinjected to the site of the bead implantation every 24 hrs by means of a glass micro-needle. Subsequently skin was collected and inverted for whole-mount analysis of hair regeneration patterns around the control beads and beads with Wnt3a or Dkk1.

**Analysis of whole-mount lacZ staining patterns.** Skins from the entire body of *BAT-gal*, *cond-lacZ* and *cond-lacZ;K14-Wnt7a* mice were collected and whole-mount X-gal staining was performed. After staining, skin samples were de-hydrated in serial dilutions of EtOH and then re-hydrated. This was done to remove subcutaneous adipose tissue and expose telogen hair follicles for subsequent analysis and photography of lacZ staining patterns.

**Predictive modeling of hair regeneration behavior.** We performed predictive mathematical modeling of the regeneration dynamics among hair stem cell clusters using a Cellular Automaton (CA) model. The patterning field is divided up into a number of

square “cells” known as automata; they can be thought of as units which exhibit programmed responses to different signals. In our model, each automaton represents a single hair stem cell cluster (mouse, human) or all hair stem cell clusters of one compound follicle unit (rabbit) as it cycles through the following successive phases: signal propagating (**P**) and non-propagating phases (**A**), and phases refractory (**R**) and competent (**C**) to such signals. Each automaton remains in a given phase for a variable interval of time after which it moves to the next state.

Our CA model is constructed from a series of assumptions that are laid out below.

**Domain.** The domain is supposed to be rectangular and a grid is imposed on the domain with **nx** automata in a vertical direction and **ny** automata in a horizontal direction.

**Time.** Time is supposed to evolve in a series of discrete steps, each of equal length, **step**. The simulation runs until time **T** hours, hence using **T/step** steps in total (if the result is not an integer, then it is rounded up to the next time step).

**States.** Automata can be in one of four phases (*aka* steps):

- **Competent (C):** automata in this state are competent to enter the **P** state if triggered to do so.
- **Propagating (P):** automata in this state are able to influence surrounding **C**-automata to enter **P** state.
- **Autonomous (A):** automata in this state do not influence surrounding automata and cannot be influenced themselves.
- **Refractory (R):** unlike **C**-automata, automata in this state cannot be induced by **P**-automata to enter **P** state.

Automata cycle through the states above. Times spent in the phases **P**, **A** and **R** are distributed according to a Gamma distribution with specified mean and variance. The time spent in **C** is dependent on intrinsic and extrinsic signals. An automaton cannot re-enter **P** unless its neighboring environment displays certain behaviors: a supra-threshold stimulus is needed for the transition from **C** to **P** and the stimulus can arise in two different ways. Firstly, we assume that **C**-automata can spontaneously gain the ability to re-enter **P** and when they do so, they send out a stimulus. However, a sufficient number of neighboring automata must also spontaneously re-enter **P** to force the stimulus above threshold levels. Secondly, we assume that automata in **P** send out stimuli: an automaton in **C** can respond to such signals, but a certain number of its neighbors must be in **P** for an automaton to receive a large enough stimulus to re-enter **P** itself. If neither of the above criteria are satisfied then an automaton remains in **C**.

Details of the algorithm are outlined in more detail below.

**Competent (C).** From this state, automata can enter **P** via one of two routes. The first depends on signals intrinsic to the automaton: at every time step, an automaton has a certain probability, **1-rnd\_th**, of becoming able to spontaneously enter **P**. It retains this

ability for a period of time chosen from a Gamma distribution with mean **meanS** and standard deviation **sdS**. If at least **sp\_th** of its neighbors also have this ability or are already in **P**, then an automaton will enter **P**. The second way in which an automaton may enter **P** is if it is induced to do so via external signals: if at least **p\_th** of its neighbors are in **P**, then an automaton enters **P**. The definition of “neighbor” is an automaton lying in the Moore neighborhood – the eight surrounding automata.

**Propagating (P).** When automata in **C** receive a supra-threshold signal they enter **P**, where they become able to influence other **C**-automata. The length of time spent in this state is also randomly selected from a Gamma distribution, but with mean **meanP** and standard deviation **sdP**. After the specified time automata enter autonomous state (**A**).

**Autonomous (A).** When automata leave **P** they enter **A**, and cannot be influenced by surrounding automata. The length of time spent in this state is also randomly selected from a Gamma distribution, but with mean **meanA** and standard deviation **sdA**. After the specified time automata enter the refractory state (**R**). If there is no autonomous state, **meanA** and **sdA** are set to zero and this phase is skipped.

**Refractory (R).** When automata leave **A** they enter **R** and cannot be influenced by surrounding automata. The length of time spent in this state is also randomly selected from a Gamma distribution, but with mean **meanR** and standard deviation **sdR**. After the specified time automata enter competent state (**C**) and the cycle begins once again.

**Gamma distribution.** The Gamma distribution is given by

$$f(x; k, \theta) = x^{k-1} \frac{e^{-x/\theta}}{\Gamma(k)\theta^k}$$

where  $k$  and  $\mu$  are positive parameters. It has mean  $\mu = k\theta$  and variance  $\sigma^2 = k\theta^2$ . This implies for **P**, for example,  $\mu = \text{sdP}^2/\text{meanP}$  and  $k = \text{sdP}^2/\text{meanP}^2$ . Since we work with discrete times, the length of time spent in each state is rounded to the nearest integer value.

**Updating.** At every time step the state of each automaton is updated: the update order is specified by creating a new random permutation of the automata at each step.

**Initial states.** Unless otherwise stated, all automata are initially taken to be in **C**.

**Boundary conditions.** Absorbing boundary conditions are applied on each edge of the grid: an extra layer of automata is added to each edge and these automata are maintained in **C**.

**Computation.** The procedure was implemented in C++ with each automaton represented by an object with two variables: the current state and the amount of time before the state was due to change. A class consisting of a two-dimensional array of objects was used to represent the field. This class contained parameter variables, the afore-mentioned field of “cells”, a variable keeping track of the number of generations the field of “cells” had passed through, and the following groups of functions:

- functions to read/write to the automaton objects;
- functions that recorded the state of the entire field of automata;
- functions that checked and applied boundary conditions;
- functions that calculated the number of nearest neighbors of a particular state a given “cell” had;
  - functions to measure and record the fractal dimension of the pattern present at a given generation;
  - functions that read and adjusted the parameters;
  - functions that updated the field according the model rules.

A set of utility functions was used to generate random calls from gamma and uniform distributions and to create ppm image files given rgb values. The movies were created by converting the ppm images to bmp images and using QuickTime software.

**Parameters.** The simulation parameters, their definitions and the values commonly used in numerical simulations are given in Table 1 below.

**Data representation.** The grid of automata states is plotted over time and the sequence of plots is converted to a movie file. Two types of plots are stored: the first shows each state as a different color (**P** – blue, **A** – yellow, **R** – red, **C** – green) whilst the second shows expected pigmentation states as they would appear on the skin (**P** – grey, **A** – black, **R** and **C** – white). In every simulation the state of the field was recorded at four-hour intervals and movies were created at 15 frames per second.

**Supplementary Table 1. Parameters used in the model simulations.**

Parameter	Description	Balanced activator/inhibitor	Activators↑	Activators↑↑	Activators↑↑
<b>Nx</b>	Number of automaton rows	80	80	80	400
<b>Ny</b>	Number of automaton columns	80	80	80	400
<b>step</b>	Number of hours per time step	4 hours	4 hours	4 hours	4 hours
<b>T</b>	Total duration of simulation	100-200 days	100-200 days	100 days	100-300 days
<b>meanP</b>	Mean time spent in <b>P</b>	4.0 days	4.0 days	14.0 days	30.0 days
<b>sdP</b>	Standard deviation of times spent in <b>P</b>	0.5 days	0.5 days	0.5 days	0.5 days
<b>meanA</b>	Mean time spent in <b>A</b>	10.0 days	10.0 days	0.0 days	0.0 days
<b>sdA</b>	Standard deviation of times spent in <b>A</b>	1.0 days	1.0 days	0.0 days	0.0 days
<b>meanR</b>	Mean time spent in <b>R</b>	28.0 days	12.0 days	12.0 days	28.0 days
<b>sdR</b>	Standard deviation of times spent in <b>R</b>	1.0-10.0 days	1.0-10.0 days	1.0 days	1.0-15.0 days
<b>meanS</b>	Mean time spent in <b>C</b>	3.0 days	3.0 days	3.0 days	3.0 days
<b>sdS</b>	Standard deviation of times spent in <b>C</b>	1.0 days	1.0 days	1.0 days	1.0 days
<b>sp_th</b>	Min. number of neighbors to spontaneously enter <b>P</b>	4	4	2	4

<b>p_th</b>	Min. number of neighbors in $P$ to stimulate entry to $P$	3	3	2	3
<b>r_th</b>	Probability of becoming spontaneously able to enter $P$	0.992-0.995	0.992-0.995	0.998-1	0.992-0.995

**Supplementary Table 2. Parameters used in the human model simulations.**

<b>Parameter</b>	<b>Description</b>	<b>Domain 1 (Fronto-parietal)</b>	<b>Domain 2 (Occipital)</b>
<b>nx</b>	Number of automaton rows	150	
<b>ny</b>	Number of automaton columns	150	
<b>step</b>	Number of hours per time step	4 hours	
<b>T</b>	Total duration of simulation	1000 days	
<b>sp_th</b>	Min. number of neighbors to spontaneously enter $P$	0	
<b>p_th</b>	Min. number of neighbors in $P$ to stimulate entry to $P$	3	
<b>r_th</b>	Probability of becoming spontaneously able to enter $P$	0.998	
<b>1st cycle</b>			
<b>meanP</b>	Mean time spent in $P$	5.0 days	5.0 days
<b>sdP</b>	Standard deviation of times spent in $P$	0.5 days	0.5 days
<b>meanA</b>	Mean time spent in $A$	65.0 days	135.0 days
<b>sdA</b>	Standard deviation of times spent in $A$	0.5 days	0.5 days
<b>meanR</b>	Mean time spent in $R$	28.0 days	98.0 days
<b>sdR</b>	Standard deviation of times spent in $R$	0.5 days	0.5 days
<b>meanS</b>	Mean time spent in $C$	3.0 days	3.0 days
<b>sdS</b>	Standard deviation of times spent in $C$	1.0 days	1.0 days
<b>2nd cycle</b>			
<b>meanP</b>	Mean time spent in $P$	5.0 days	5.0 days
<b>sdP</b>	Standard deviation of times spent in $P$	0.5 days	0.5 days
<b>meanA</b>	Mean time spent in $A$	44.0 days	79.0 days
<b>sdA</b>	Standard deviation of times spent in $A$	0.5 days	0.5 days
<b>meanR</b>	Mean time spent in $R$	92.0 days	84.0 days
<b>sdR</b>	Standard deviation of times spent in $R$	0.5 days	0.5 days
<b>meanS</b>	Mean time spent in $C$	3.0 days	3.0 days
<b>sdS</b>	Standard deviation of times spent in $C$	1.0 days	1.0 days
<b>3rd and following cycles</b>			
<b>meanP</b>	Mean time spent in $P$	0.0 days	
<b>sdP</b>	Standard deviation of times spent in $P$	0.0 days	
<b>meanA</b>	Mean time spent in $A$	84.0 days	
<b>sdA</b>	Standard deviation of times spent in $A$	14.0 days	

<b>meanR</b>	Mean time spent in <i>R</i>	84.0 days
<b>sdR</b>	Standard deviation of times spent in <i>R</i>	14.0 days
<b>meanS</b>	Mean time spent in <i>C</i>	3.0 days
<b>sdS</b>	Standard deviation of times spent in <i>C</i>	1.0 days
<b>Cycles upon alopecia</b>		
<b>meanP</b>	Mean time spent in <i>P</i>	0.0 days
<b>sdP</b>	Standard deviation of times spent in <i>P</i>	0.0 days
<b>meanA</b>	Mean time spent in <i>A</i>	7.0 days
<b>sdA</b>	Standard deviation of times spent in <i>A</i>	0.5 days
<b>meanR</b>	Mean time spent in <i>R</i>	336.0 days
<b>sdR</b>	Standard deviation of times spent in <i>R</i>	0.5 days
<b>meanS</b>	Mean time spent in <i>C</i>	3.0 days
<b>sdS</b>	Standard deviation of times spent in <i>C</i>	1.0 days

To simulate human hair regeneration, the patterning field was divided into two domains: domain 1 (upper 2/3) representing the fronto-parietal scalp, and domain 2 (lower 1/3) representing the occipital scalp. Automata in each domain behave according to the parameters specified in the table above. These parameters are derived from known regeneration behavior of scalp hair follicles during 1<sup>st</sup> and 2<sup>nd</sup> fetal growth cycles (Cutrone and Grimalt, 2005; Halloy 2000), as well as during normal adult growth cycles and growth cycles upon alopecia.

**Supplementary Table 3. Percentage of telogen hair follicles (HF) with spontaneous WNT activity in dermal papillae during *R-phase* and *C-phase*.**

Mice	Solitary HFs	Groups of 2 HFs	Groups of 3 HFs	Groups of 4 HFs	Groups of 5+ HFs
<i>BAT-Gal</i>	0.18%	0%	0%	0%	0%
	4.89%	0.23%	0.03%	0.01%	<0.01%
<i>Cond-lacZ</i>	0.10%	0%	0%	0%	0%
	4.98%	0.16%	0.06%	0.02%	<0.01%
<i>Cond-lacZ; K14-Wnt7a</i>	~100% WNT-active ~100% WNT-active				

**Supplementary Figure Legend**

**Supplementary Figure 1. (A) Spatio-temporal coupling between follicular stem cell activation and follicular pigmentation.** In dormant telogen follicles the epithelial progenitor population consists of bulge stem cells and hair germ cells. At the very beginning of anagen, hair germ progenitor cells are the first to be activated. Their proliferation sustains initial down-growth of the follicle during early anagen. Two days later a portion of bulge stem cells also activate and proliferate (Greco *et al.* 2009 Cell

Stem Cell, 4:155-69). About the same time, pigmentation starts within the newly formed bulb of the hair follicle. This results in very close temporal coupling of follicular stem cell activation and the initiation of follicular pigmentation. This can be easily observed at later times through the skin surface.

**(B) Cellular Automata framework.** Predictive mathematical modeling of the regeneration dynamics among hair stem cell clusters was performed using Cellular Automaton model. In this model the rectangular patterning field is divided up into a number of square “cells” known as automata. The eight automata surrounding one automaton are defined as its neighbors. In our model, each automaton represents a single hair stem cell cluster (mouse, human) or all hair stem cell clusters of one compound follicle unit (rabbit) as it cycles through the following successive phases: signal propagating (*P*) – blue, and non-propagating phases (*A*) - yellow, and phases refractory (*R*) – red, and competent (*C*) - green, to such signals. Each automaton remains in a given phase for a variable interval of time after which it moves to the next state. Automata in certain states can interact: *C*-automata are competent to enter the *P* state if triggered to do so. *P*-automata are able to influence surrounding *C*-automata to enter *P* state (white arrows and thick white borders). *A*-automata do not influence surrounding automata and cannot be influenced themselves (white stop signs and thick black borders). *R*-automata unlike *C*-automata cannot be induced by *P*-automata to enter *P* state (white stop signs and thick black borders).

**Supplementary Figure 2. Predictive modeling of the regeneration dynamics among hair stem cell clusters with balanced activator/inhibitor levels.** (A) Wave spreading. (B) Initiation events. (C) Border stability. (D) Border instability. Two types of plots are shown: the left-hand plot shows each state as a different color (*P* – blue, *A* – yellow, *R* – red, *C* – green) whilst the right-hand plot shows expected pigmentation states as they would appear on the skin (*P* – grey, *A* – black, *R* and *C* – white). Each plot set is labeled with the number of days simulated. Movie **S1** accompanies (A), movie **S2** accompanies (B), movie **S3** accompanies (C) and movie **S4** accompanies (D). More information on the CA modeling procedure can be found in the Material and Methods.

**Supplementary Figure 3. Predictive modeling of the regenerative patterns upon progressive increase in activator levels.** The CA model predicts faster global regeneration dynamics when the parameters of the automaton cycle are adjusted to reflect progressive rise in activators: (B, E) duration of *R*-phase is shortened; (C, F) duration of *R*-phase is shortened, duration of *P*-phase is increased at the expense of *A*-phase, minimal number of neighboring automata required to spontaneously enter *P*-phase is reduced and probability of spontaneous *P*-phase entry is increased. Movies **S5** and **S6** accompany this figure. Also, see **Supplementary Table 1**.

**Supplementary Figure 4. Predictive CA modeling of the interaction between fast and slow patterns.** (A) Large-scale (400x400 automata) CA modeling of the regenerative patterns resulting from the rise in hypothetical activators (see **Supplementary Table 1**). Multiple spontaneous *C*→*P* initiation events occur and multiple continuous *C*→*P* spreading waves exist simultaneously. As modeling time increases, complex, fractal patterns develop. Movie **S7** accompanies this figure. (B) CA

modeling of the interaction between slow (balanced activators / inhibitor profile) and fast (more activation) patterning fields: the top plot shows each state as a different color ( $P$  – blue,  $A$  – yellow,  $R$  – red,  $C$  – green) whilst the bottom plot shows expected pigmentation states as they would appear on the skin ( $P$  – grey,  $A$  – black,  $R$  and  $C$  – white). Movie **S8** accompanies this figure.

**Supplementary Figure 5. Predictive expression profiling of skin macro-environment for new diffusible modulators.** Modeling using CA framework predicts high expression levels of inhibitory pathway ligands and activating pathway antagonists in the  $R$ - vs.  $C$ -phase of telogen and also in the  $A$ - vs.  $P$ -phase of anagen. We looked for expression patterns that match these predictions to identify new macro-environmental modulators of hair regeneration. We confirm *Bmp2* as the key inhibitory pathway ligand (**A**). We also identify *Dkk1* and *Sprf4* as the new macro-environmental modulators that antagonize Wnt signaling (**C, D**). Both of these soluble Wnt antagonists are expressed in the skin macro-environment during  $R$ - and  $A$ -phases and are absent during  $C$ - and  $P$ -phases. (**E**) Each of the four  $P \rightarrow A \rightarrow R \rightarrow C$  phases has unique Wnt/Bmp expression profile.

**Supplementary Figure 6. Real regenerative patterns in *K14-Nog* and *K14-Wnt7a* transgenic mice.** In comparison with WT mice (**A, B**) *K14-Nog* mice, that over-express Bmp antagonist noggin, display very short telogen, continuous propagation of anagen waves and lack of stable anagen-telogen borders. Hair cycle patterns in *K14-Nog* mice are simplified and very dynamic (**C**). *K14-Wnt7a* mice, that over-express Wnt7a, display significantly shortened telogen, continuous propagation of anagen waves and lack of stable anagen-telogen borders (**D-F**). Hair cycle patterns in *K14-Wnt7a* mice are more intricate and more dynamic than in WT mice (**E, F**). In addition, the telogen skin of *K14-Wnt7a* mice has many more spontaneous anagen initiation sites (see Fig. **2F** and fig. **S10B-C**). These changes in regeneration patterns in *K14-Nog* and *K14-Wnt7a* transgenic mice reflect progressive rise in activators predicted by the CA model on fig. **S3**. Scale bars: 5 cm.

**Supplementary Figure 7. Modulation of hair wave patterns with Wnt3a and Dkk1.** In bead implantation experiments, administration of Wnt3a protein causes premature anagen initiation in surrounding telogen hair follicles (**B, E**), while administration of Dkk1, a Wnt antagonist, prevents normal progression of the physiological anagen spreading wave (**C, F**). Control BSA beads have no effect on regenerative patterns (**A, D**). Red dotted outlines on **B, E, F** mark boundaries between anagen and telogen skin; white arrows on **E** and **F** show direction of anagen spreading waves.

**Supplementary Figure 8. Involvement of Wnt signaling in spontaneous anagen initiation.** (**A-F**) In *BAT-gal* and *cond-lacZ* WNT reporter mice spontaneous WNT activity (blue color) occurs in dermal papillae of  $C$ -phase (Wnt-ON), but not of  $R$ -phase (Wnt-OFF) telogen hair follicles (micro-dissected telogen hair follicles are shown on **C** – *BAT-gal* and on insert on **F** – *cond-lacZ*). Note that constitutive reporter activity is also seen in *cond-lacZ* follicles in the isthmus area). Wnt-ON dermal papillae in  $C$ -phase are distributed sporadically and represent only ~5% of all telogen hair follicles. While most of them are solitary, in rare occasions they form groups (see **Supplementary Table 3**).

**(J)** Only groups of at least five Wnt-ON dermal papillae lead to stimulation of adjacent stem cells and formation of a new anagen initiation center. **(I, K)** Within an anagen spreading wave (i.e. facilitated  $C \rightarrow P$  transition) WNT activity is observed in nearly 100% of dermal papillae ahead of the wave front. This WNT activity in dermal papillae precedes WNT activity within the hair germ (part of the progenitor cell cluster). **(L)** The number of WNT active dermal papillae does not increase within *C*-phase telogen skin along the anagen/telogen (*A*-phase/*C*-phase) border in *cond-lacZ* mice. This lack of elevated WNT activity contrasts that in anagen spreading waves (*P*-phase/*C*-phase) and is likely due to the inhibitory effect of *Dkk1* and *Sfrp4* WNT antagonists that are expressed in *A*-phase anagen skin (see fig. **S5C, S5D**). Constitutive over-expression of *Wnt7a* in *cond-lacZ;K14-Wnt7a* mice likely negates this inhibitory effect of *Dkk1* and *Sfrp4*, causes dermal papillae to become constitutively WNT active both in *C*- and *R*-phases (**G, H**) and prevents the formation of stable anagen/telogen borders (**L**). **(M)** Model of macro- and micro-environment mediated activation of hair follicle stem cells. 1) In the *R*-phase of telogen WNT antagonists, such as *Dkk1* and *Sfrp4*, and inhibitory *Bmp2/4* ligands collectively keep hair follicle stem cells in a quiescent state; 2) Loss of these WNT antagonists from the macro-environment in the *C*-phase of telogen enables spontaneous, low-frequency WNT activity in the dermal papillae; 3) Rare, probabilistic occurrence of large groups of simultaneously WNT active dermal papillae is necessary to stimulate adjacent stem cells and to induce spontaneous  $C \rightarrow P$  activation events (i.e. new anagen initiation centers). Canonical WNT activity in dermal papillae was recently shown to be critical for anagen stimulation (Enshell-Seijffers *et al.* 2010 *Developmental Cell*, 8:633-42). Secondary signaling factors (such as *Fgf7/10*) are likely produced by WNT active dermal papillae. These secondary factors directly stimulate hair follicle stem cells and induce anagen initiation (Greco *et al.*, 2009; Enshell-Seijffers *et al.*, 2010). We argue that a large group of WNT active dermal papillae needs to arise for these secondary dermal papillae-derived signaling factors to reach threshold levels sufficient to stimulate adjacent stem cells. Most of the spontaneous WNT activation events involve less than five dermal papillae and do not produce above-threshold activation signaling. Thus, skin macro-environment provides continuous areas of BMP and WNT signaling. Continuous macro-environmental WNT signaling is interpreted by individual, evenly distributed dermal papillae (part of the micro-environment), that generate secondary, short-range signaling cues (*Fgf7/10*) to adjacent stem cells clusters. This *macro-* to *micro-*environment signal translation provides a biological basis for the CA-like behavior observed in the large-scale hair regeneration system.

**Supplementary Figure 9. Long term follow-up of regenerative patterns in rabbits.**

Rabbits form complex hair regenerative patterns characterized by multiple spontaneous initiation centers, many simultaneous spreading waves and intricate fractal-like shapes. The temporal progression of dorsal patterns is shown. Often in rabbits, anagen/telogen borders are not stable. They continuously move into *C*-phase telogen territories (track the changes in the bulge-like shape indicated by a red arrowhead on **G** from day 0 to day 35). Similarly, continuous border changes can be seen on **H** from day 7 to day 28. However, when neighboring telogen skin is in *R*-phase, anagen domain borders can remain stable for prolonged periods of time (from day 64 to day 78 on **H**). Scale bars: **A-E**, 5 cm; **F-H**, 1 cm.

**Supplementary Figure 10. Microscopic basis of regenerative patterns in mice and rabbits.** (A-F) All hair regenerative events (initiation, spreading, non-percolating and percolating borders) can be observed at the microscopic level as interactions between individual hair follicles. Skin samples were inverted to reveal pigmented anagen hair follicles. Telogen hair follicles that lack pigmentation are not obvious. *K14-Wnt7a* mice display largely de-regulated patterns (B, C) that bear close resemblance to patterns in rabbits (D-F). Both *K14-Wnt7a* mice and rabbits display percolating, intricate domain boundaries (red and green dotted outlines) and multiple spontaneous initiation centers (yellow arrows or yellow outlines). (G-V) Diversity of initiation events and spreading waves in rabbit skin. In rabbit, spontaneous  $C \rightarrow P$  initiation events (G-J) and facilitated  $C \rightarrow P$  activation from the border with anagen hair follicles (K, L) are equally prevalent. Two types of spontaneous initiation centers can be found: large (G) and micro-sized (H). While spontaneous initiation centers can induce new anagen independent of each other (G H), often clusters of closely positioned initiation centers act cooperatively (I, J). It is common to observe as many as tens, and even hundreds, of micro-sized initiation centers activating large areas of  $C$ -phase telogen skin simultaneously (J). Facilitated  $C \rightarrow P$  activation from the border can be centrifugal (K) or centripetal (L). It is usual to observe complex initiation events, where both spontaneous and border-facilitated  $C \rightarrow P$  activations occur side-by-side (M-O). (P) Initial  $C \rightarrow P$  activation from spontaneous initiation centers (red arrow at day 0) can be followed by secondary activation from the border (green open arrow at day 15). (Q-S)  $C \rightarrow P$  spreading waves can be non-percolating (spreading as a smooth wavefront, Q) as well as percolating (R, S). In the case of percolating spreading, it appears that anagen attempts to spread into telogen skin, but eventually fails (red arrowheads on R and S) resulting in branch-like shapes. Anagen can only spread into  $C$ -phase telogen skin. This can be observed as unidirectional spreading from the thin border (red arrows on T-V). Blue and red arrowheads – activation from the border; green arrowheads – activation by large spontaneous centers; yellow arrowheads – activation by micro-sized spontaneous centers; red arrows – direction of anagen spreading wave. Scale bars: G-V, 1 cm.

**Supplementary Figure 11. Histology and molecular expressions in hair regenerative wave in rabbits.** (A-C) Sequential anagen initiation within compound hair follicles units in rabbit. Individual follicles within the compound unit in rabbit enter anagen sequentially, rather than in synchrony. Typically, there may be several leading follicles that enter anagen initially. The remaining follicles enter anagen at various time points. It is common to find compound units with anagen, early anagen, very early anagen and telogen hair follicles present at the same time (C). (D) PcnA immuno-staining reveals the complex dynamics of proliferation in various compartments of rabbit skin (epidermis, hair follicle epithelium, dermal cord). The relative timing of PcnA expression in various compartments is represented by colored lines. A transient increase in proliferation in interfollicular epidermis and dermal cords accompanies anagen initiation. (E) Nuclear  $\beta$ -catenin is absent in telogen and appears first during very early anagen in the epithelial compartment of rabbit hair follicles (green arrowheads). In developed anagen hair follicles, nuclear  $\beta$ -catenin is abundant in epithelial matrix. The relative timing of epithelial cytoplasmic and nuclear of  $\beta$ -catenin expression is represented by colored lines.

Nuclear  $\beta$ -catenin is also detected in dermal papilla cells. **(F)** In rabbit skin, *Bmp2* is differentially expressed in dermal cord adipocytes. *Bmp2* is high in early, R-phase telogen and low or undetectable in late, C-phase telogen. *Bmp2* expression is very patchy and generally low throughout the entire anagen and catagen phases. The relative levels and timing of *Bmp2* expression are represented by color lines.

**Supplementary Figure 12. Summary diagram of rabbit skin anatomy.** Rabbits have compound hair follicle units, meaning that each compound unit is composed of multiple individual follicles sharing one or a few closely apposed orifices, yet with each follicle having a separate cluster of stem cells, matrix, and dermal papilla (each compound unit here is represented as a group of three follicles). This is in contrast to mice in which each hair follicle is simple, with one bulge and one dermal papilla. Despite close morphological proximity, rabbit hair follicles within the compound unit enter anagen sequentially rather than in synchrony (see second and third compound units). Also, subcutaneous adipose tissue in rabbits is organized in discontinuous "dermal cords" surrounding each compound follicle unit (shown in yellow and red). During anagen, follicles of the compound unit extend into the lower dermis strictly along the length of the dermal cord fibers. At the same time, dermal cord adipocytes significantly enlarge. There is cyclic expression of *Bmp2* in these dermal cord adipocytes (*Bmp2* is expressed in red "dermal cord"). Anagen initiation in rabbit skin can occur via self-activation or via coupling between neighboring compound units (green arrows).

**Supplementary Figure 13. Long term follow up of patterning behavior upon rabbit-on-mouse skin xeno-transplantation.** Upon transplantation to mouse (albino SCID), rabbit skin (pigmented black) maintains dynamic hair growth and exhibits initiation and spreading events typical to rabbits. This includes formation of multiple spontaneous initiation centers (day 111, green arrowheads); micro-sized initiation centers (day 173 and day 186, inserts);  $C \rightarrow P$  activation from the border (day 116, red arrows). At the same time rabbit and mouse skins can communicate  $C \rightarrow P$  initiation signals across the transplant border.  $C \rightarrow P$  initiation events in rabbit skin appear to dominate and spread onto mouse skin (day 159, arrowhead – rabbit initiation center, arrow – anagen spreading wave). Green dotted lines mark anagen domains in rabbit skin; red dotted lines mark anagen domains in SCID mouse skin. Scale bar: 1 cm.

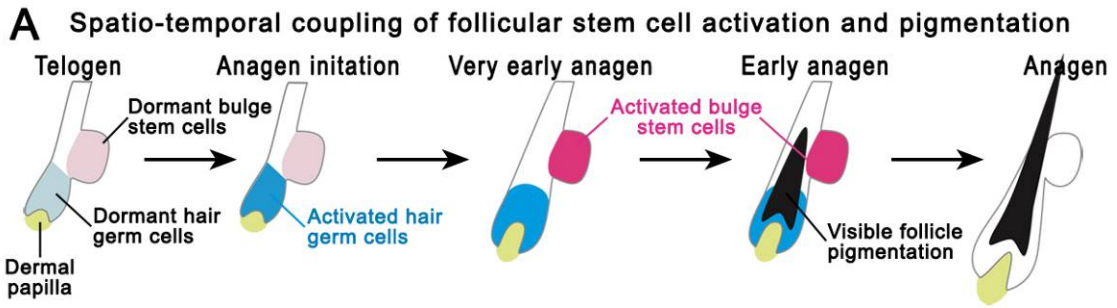
**Supplementary Figure 14. Spatial self-similarity of rabbit patterns.** Regenerative patterns in rabbits display fractal geometry and mathematical self-similarity over the spatial scale range of 4X **(B)**. Self-similarity was accessed based on the measurements of the fractal dimension,  $D$ , a mathematical measure of self-similarity. Importantly, the fractal-like patterns produced upon large-scale modeling **(A)** with parameters adjusted to reflect a rise in hypothetical activators (see fig. **S4A**) is identical to that of real rabbit regenerative patterns. This essentially confirms that overall activator levels are high in rabbit skin.

**Supplementary Figure 15. CA model simulations of human scalp hair regenerative patterns.** Human scalp hair regenerative patterns were simulated using a series of assumptions derived from known human scalp hair regenerative behavior during 1<sup>st</sup> and

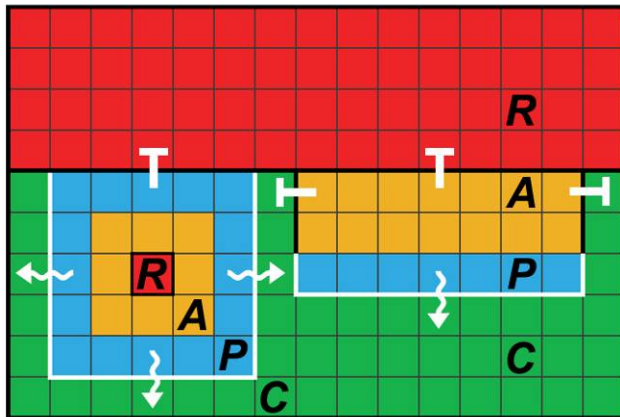
2<sup>nd</sup> fetal growth cycles (Cutrone and Grimalt, 2005; Halloy, 2000), as well as during normal adult growth cycles and growth cycles upon alopecia (see **Supplementary Table 2**). Two types of plots are shown: the right-hand plot shows each automaton state as a different color (*P* – blue, *A* – yellow, *R* – red, *C* – green) whilst the left-hand plot shows expected follicular pigmentation states as they would appear on the skin (*P* – grey, *A* – black, *R* and *C* – white). Initially all automata are in *C*-phase and several spontaneous initiation sites quickly develop (reflecting first embryonic hair growth cycle; d3.3). The differences between top (fronto-parietal) and bottom (occipital) regions of the field emerge: the top region re-enters *R*-phase (d73.3) and then *C*-phase (d101.7) more quickly and goes through another cycle (reflecting second embryonic hair growth cycle; d105.8). The top region of the field then becomes asynchronous (third postnatal hair growth cycle, d251.7). Meanwhile the bottom region of the field ends its first *A*-phase later (d144.2), re-enters the second synchronized cycle (d246.7) and eventually enters third asynchronous cycle (d410). Eventually, the differences between the top and the bottom domains disappear (d621.7). Towards the end of the simulation, parameters consistent with alopecia are implemented in a section of the top region and we see almost all follicles in *R*-phase. Movie **S9** accompanies this figure.

**Supplementary Figure 16. A unifying model of stem cell regeneration in a large population of hair follicles.** (A) The spectrum of hair regenerative patterns. (B) The spectrum of stem cell topology and hair follicle interactions. During the evolution of hair follicles, epithelial stem cells undergo topological clustering into bulges. Each such cluster can be regulated as one entity, where all stem cells either remain quiescent or become activated relatively synchronously. This allows for the conversion from the continuous renewal mode observed in epidermis to the episodic regeneration mode, such as that observed in the hair cycle. Stem cell clustering and episodic hair cycling represent evolutionary novelties and enable new ways for the large-scale coordination of regeneration. Each cluster of hair stem cells can become activated by the intrinsic hair cycle clock (Y axis on **B**). Intrinsic activation alone can ensure sufficient levels of hair regeneration if occurs with high probability. This is seen in the adult human scalp, where hair follicles regenerate autonomously based on the intrinsic activation (Y axis on **A**). Hair regeneration based on this mechanism alone can become easily deficient when the probability of intrinsic activation drops, such as upon alopecia. Additionally, this mechanism does not allow for any coordination of regeneration among neighboring hair follicles. We show that diffusible signaling molecules used for regulating hair stem cell activities within each hair follicle can be co-opted to mediate interactions between neighboring hair follicles. Such signaling couples activation events among many stem cell clusters at once (X axis on **B**). By modulating the strength of intrinsic stem cell activation (Y axis) and the probability of coupled activation (X axis), different animals or different physiological conditions in the same animal can significantly alter the global dynamics of hair regeneration. As the result, versatile hair growth patterns in rabbits, mice, normal and alopecia human scalps can be all explained within the same patterning framework which is based simply on how hair stem cell activities are “managed” (A).

# Supplementary Figure 1

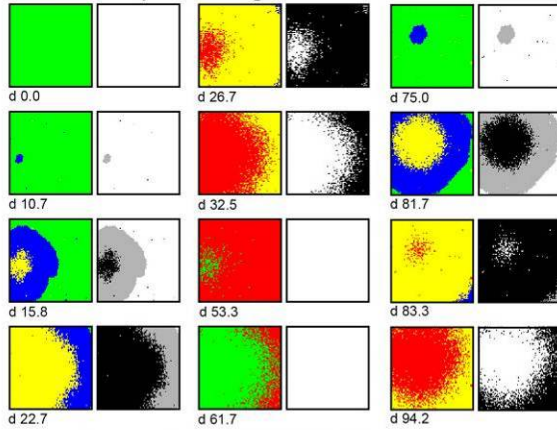


**B Cellular automata framework**

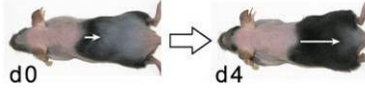


## Supplementary Figure 2

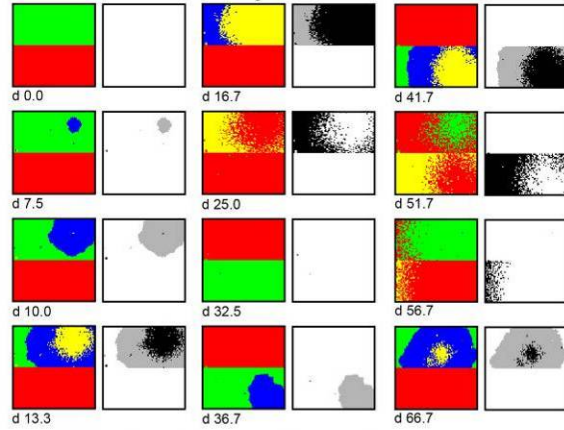
### A Wave spreading



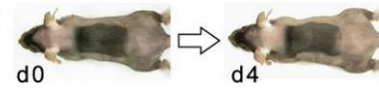
*In vivo* wave spreading



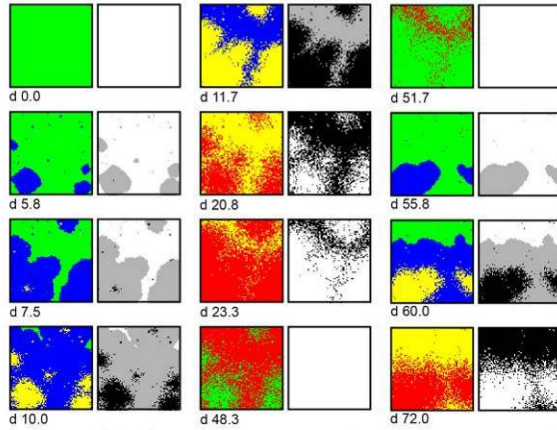
### C Border stability



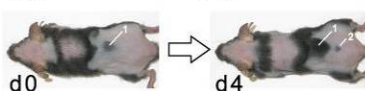
*In vivo* border stability



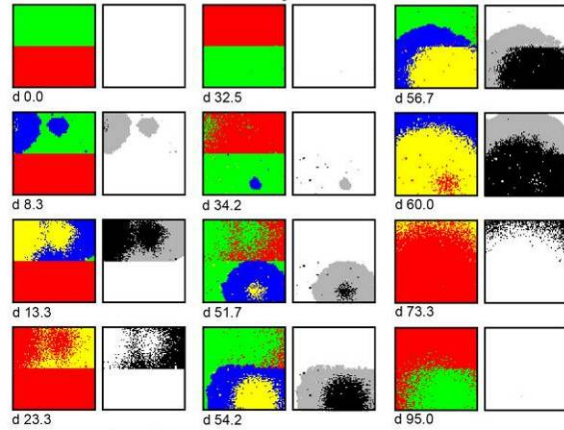
### B Initiation events



*In vivo* initiation events



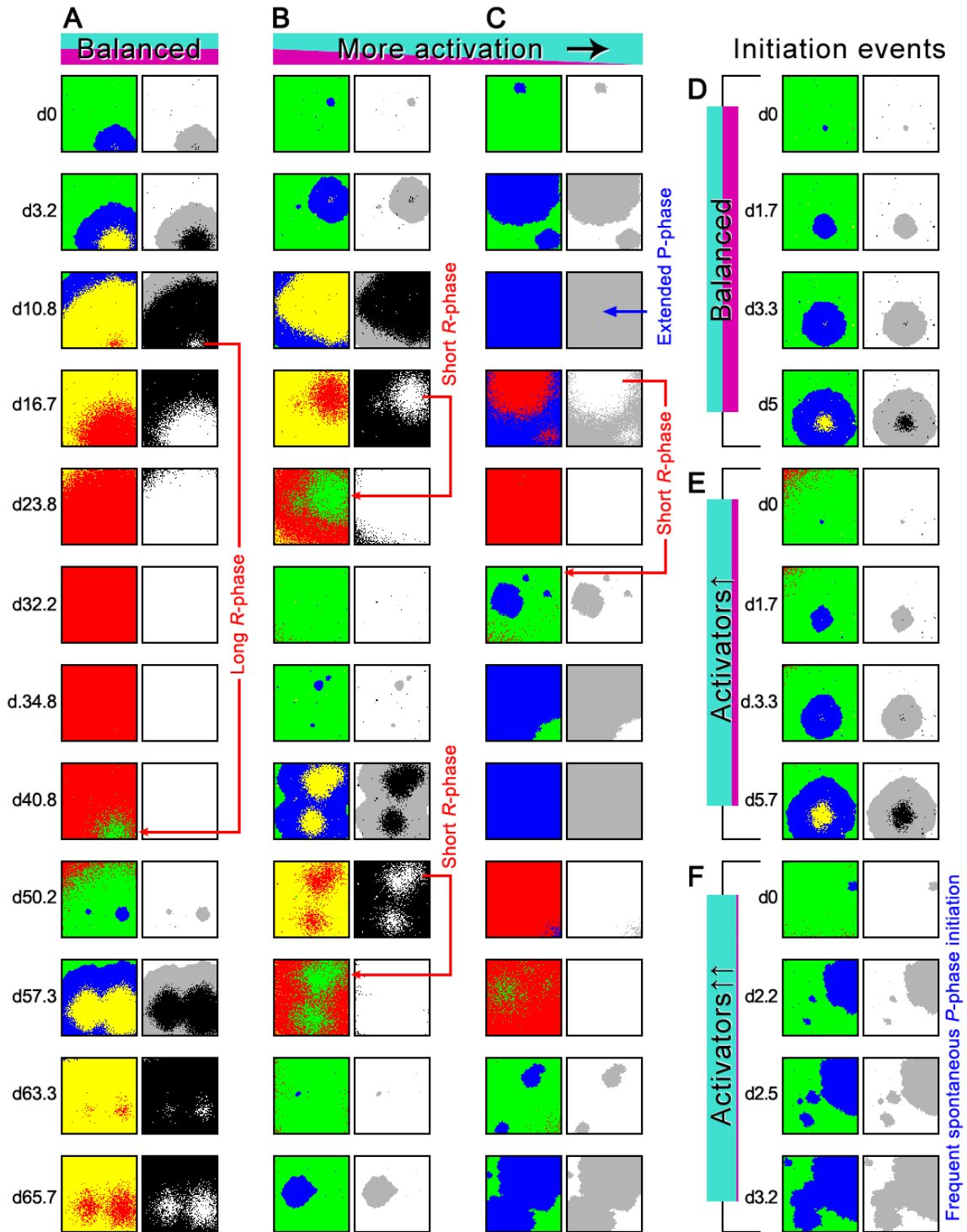
### D Border instability



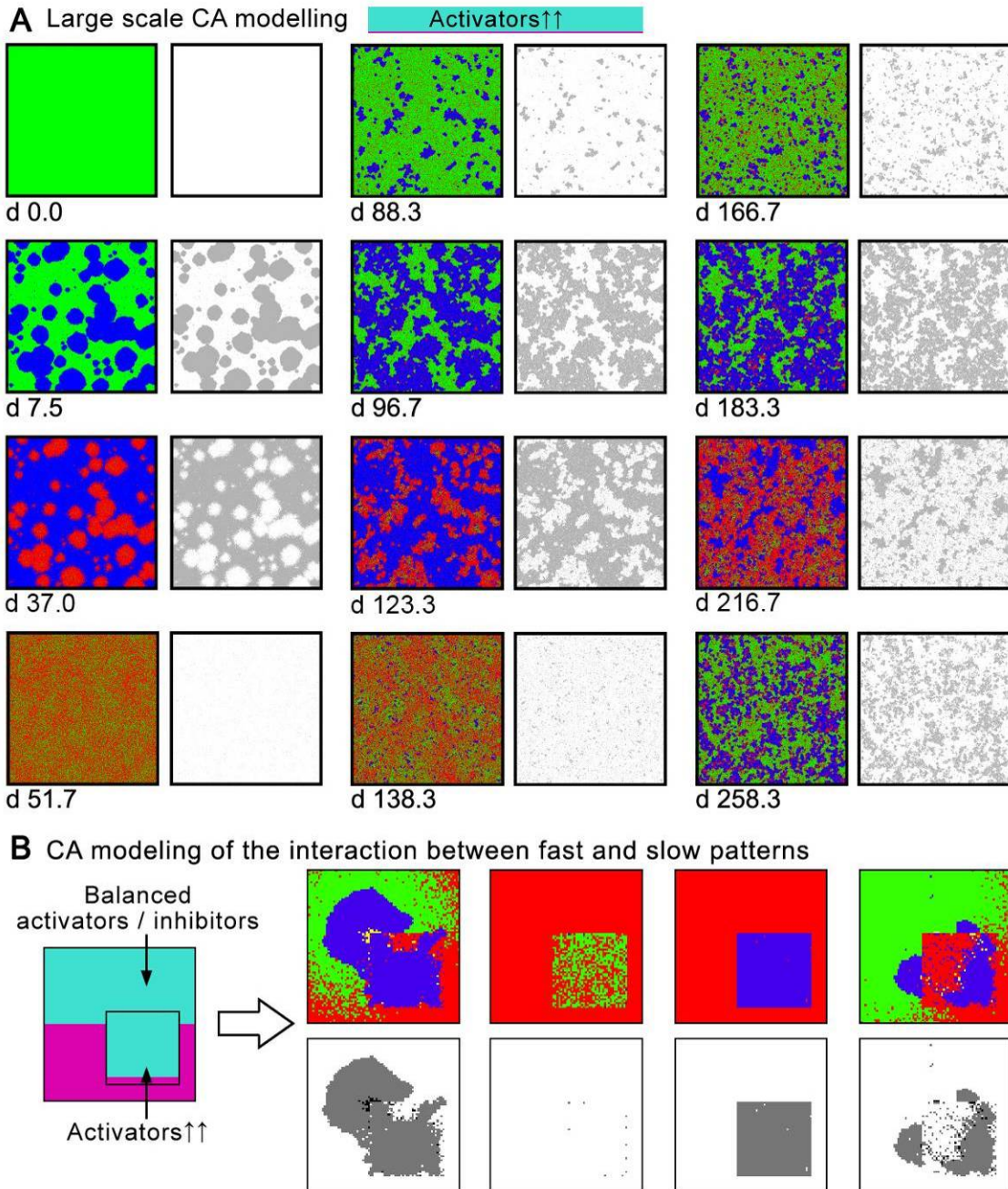
*In vivo* border instability



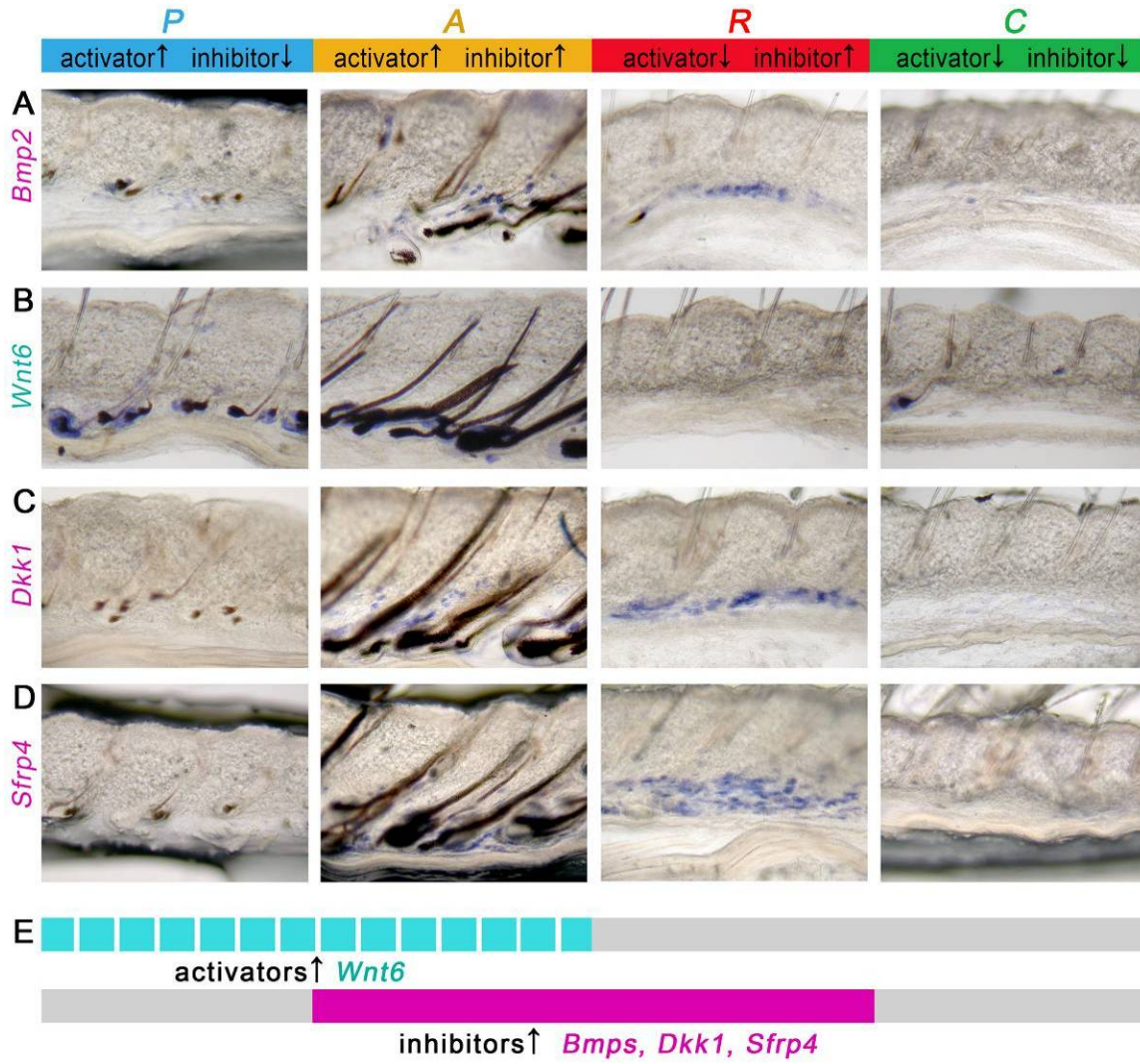
Supplementary Figure 3



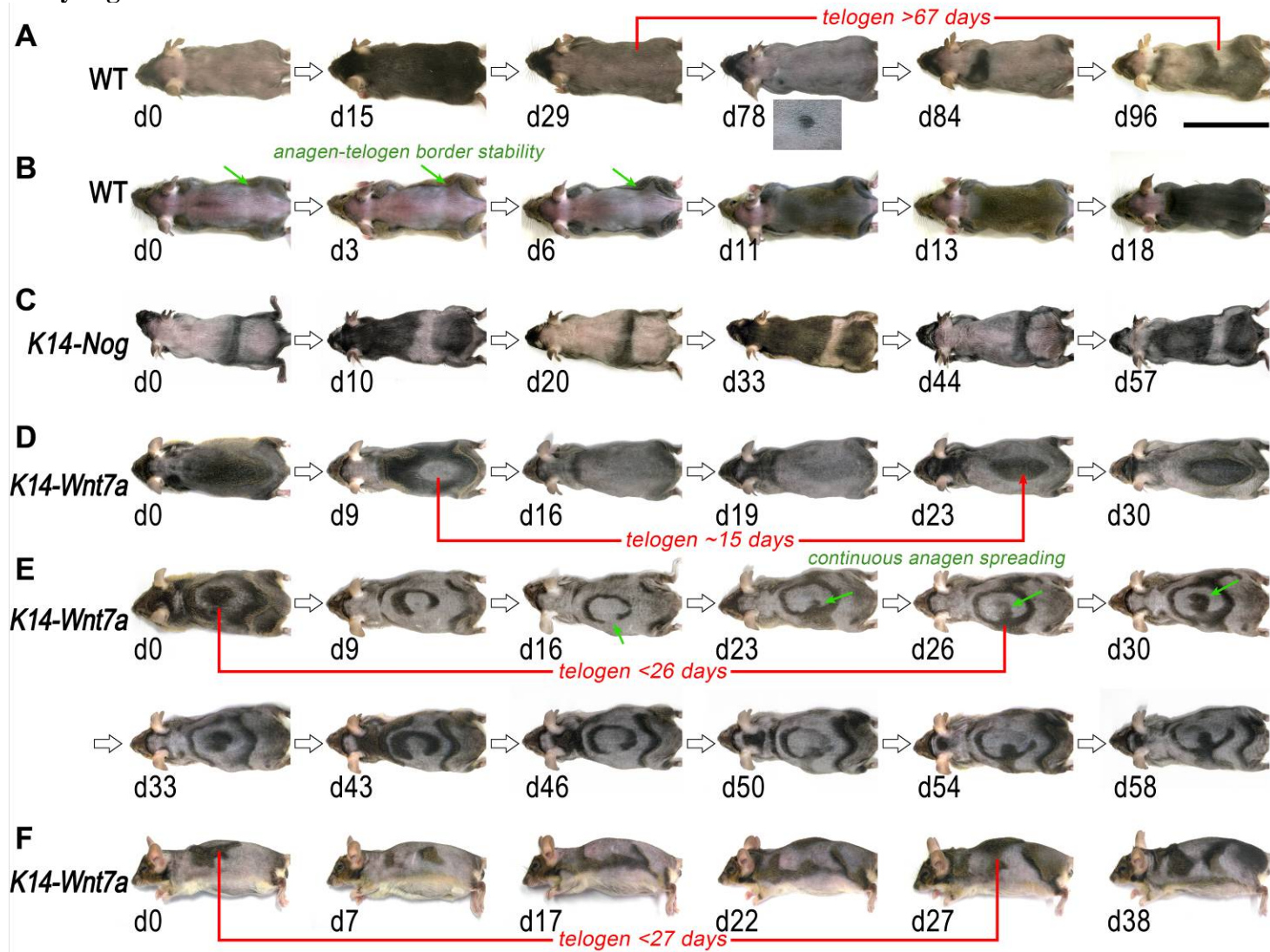
## Supplementary Figure 4



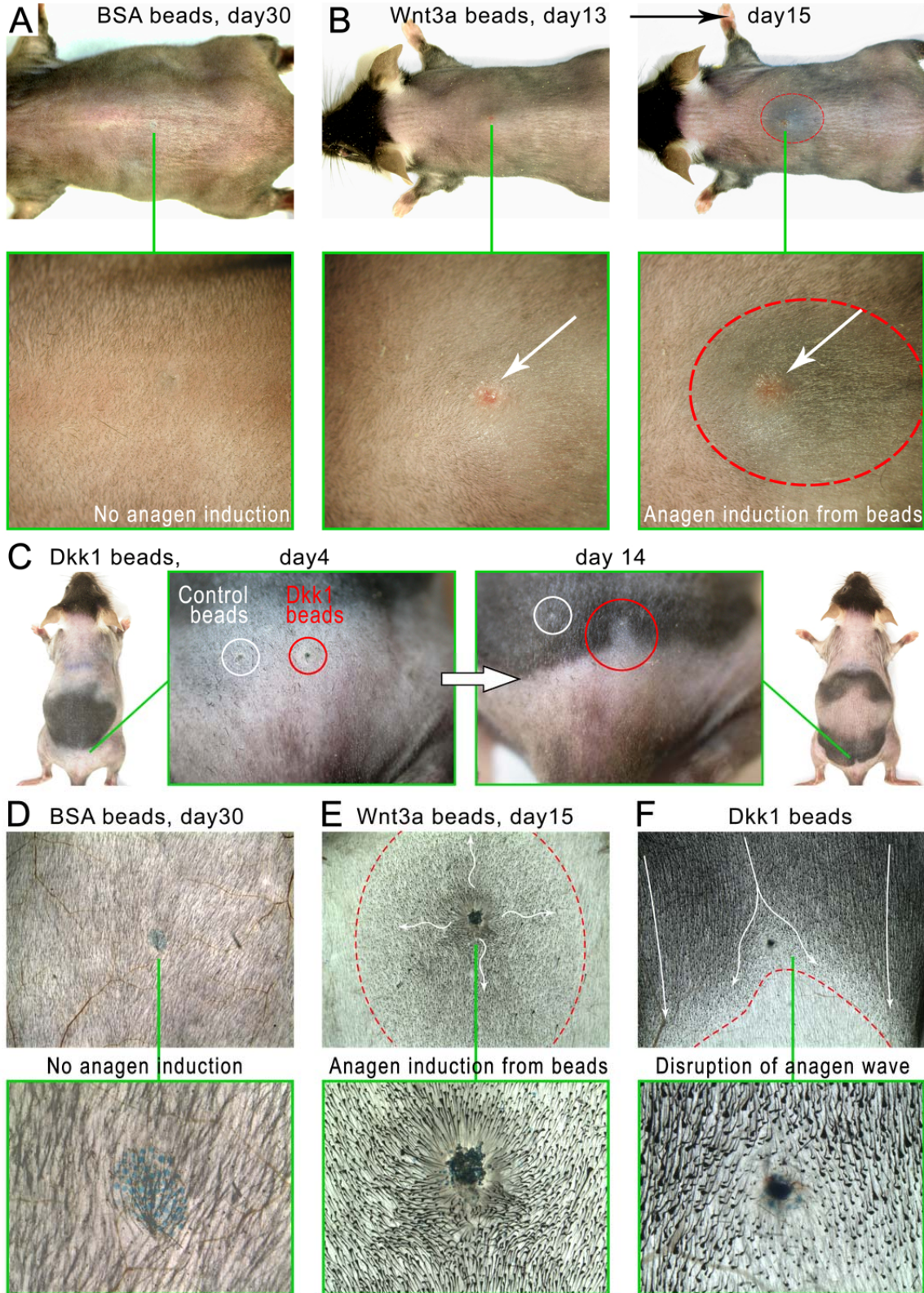
Supplementary Figure 5



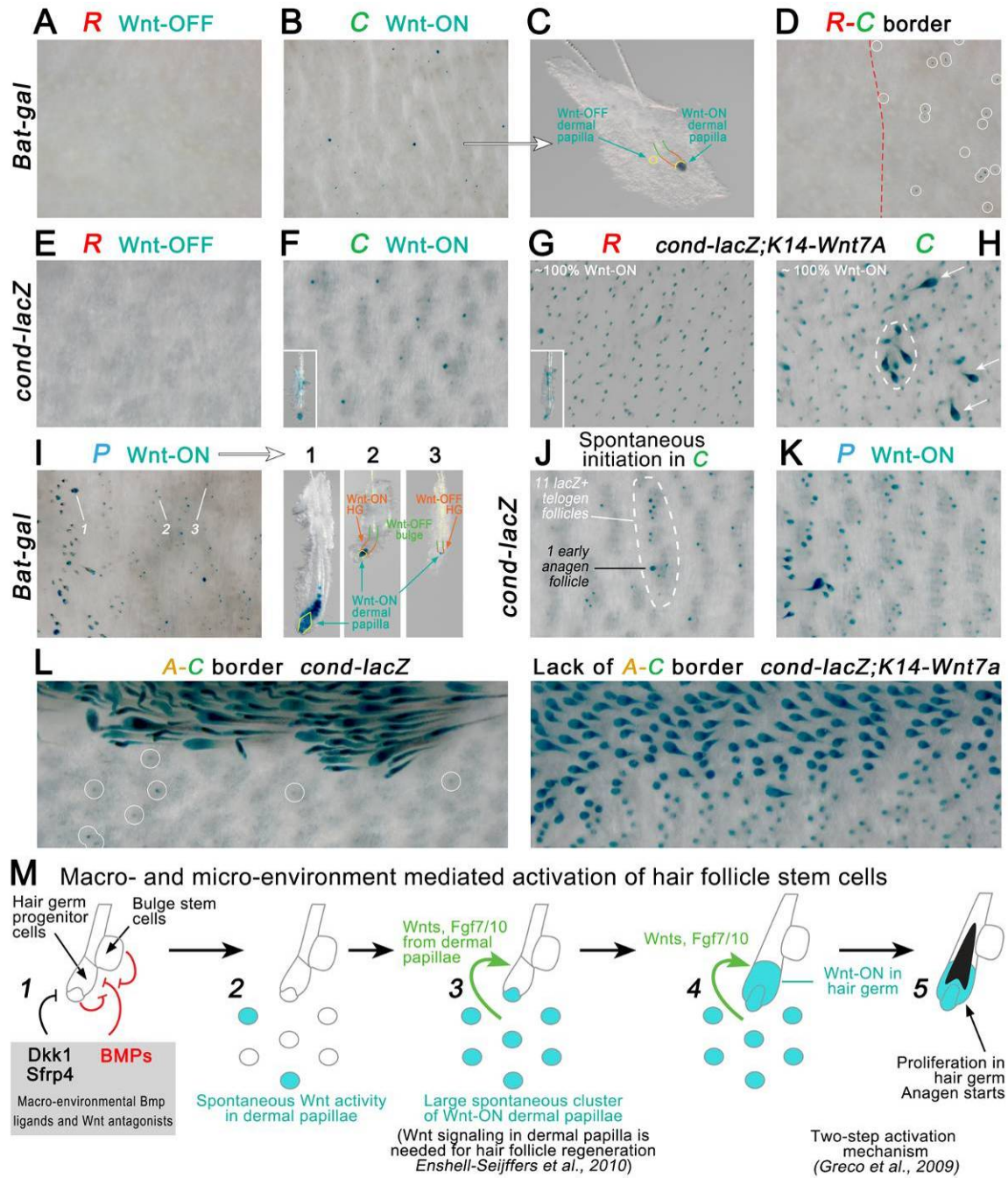
Supplementary Figure 6



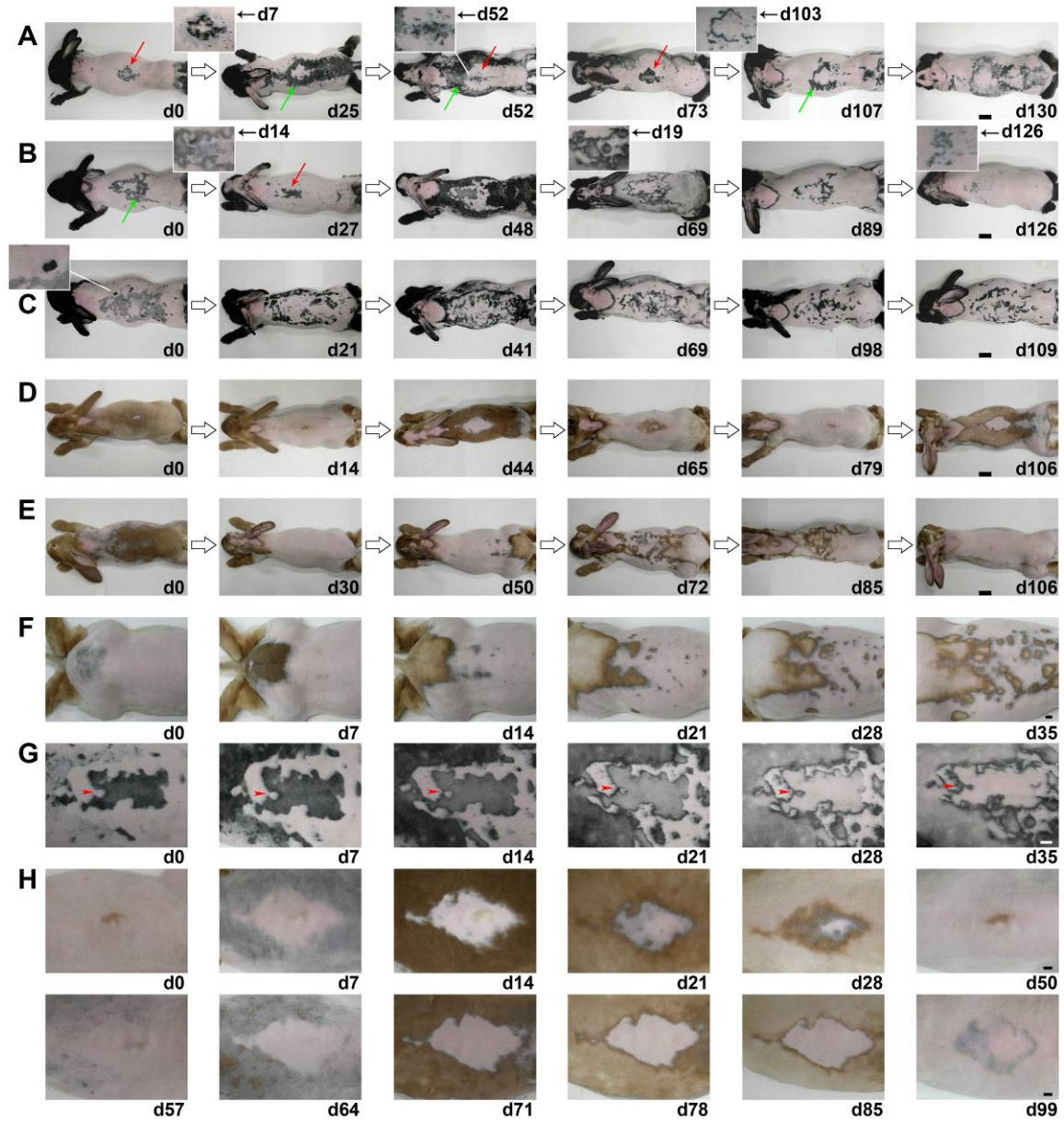
**Supplementary Figure 7**



Supplementary Figure 8

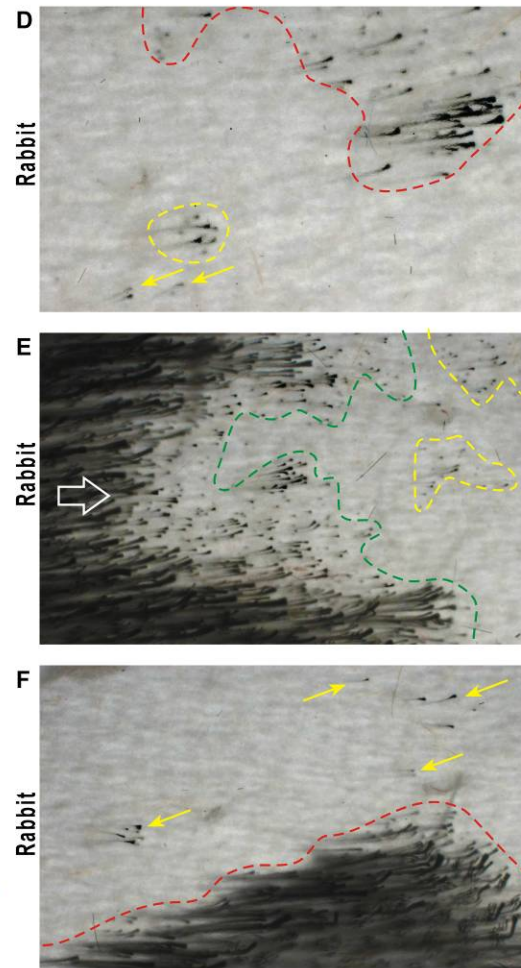
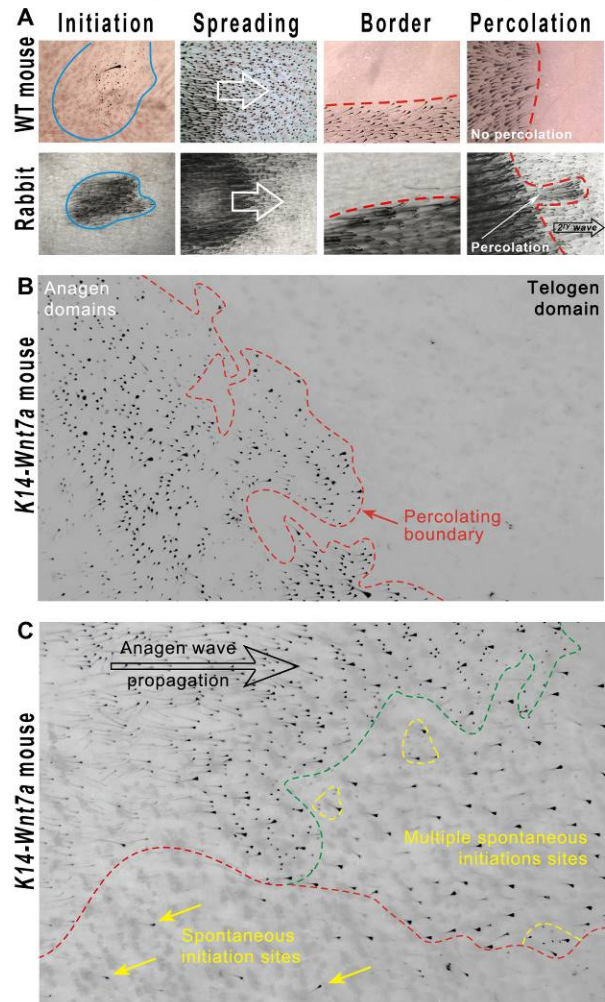


Supplementary Figure 9

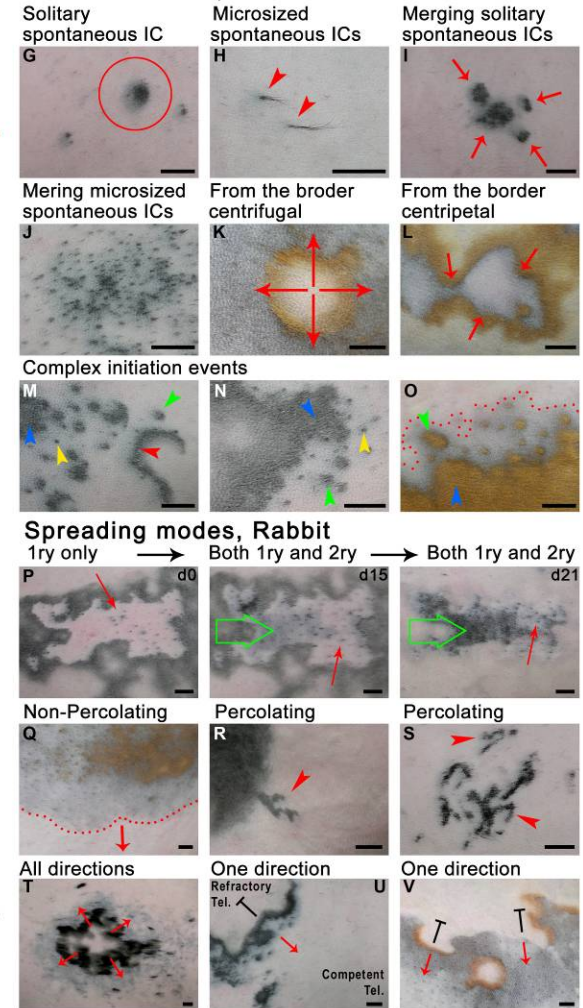


# Supplementary Figure 10

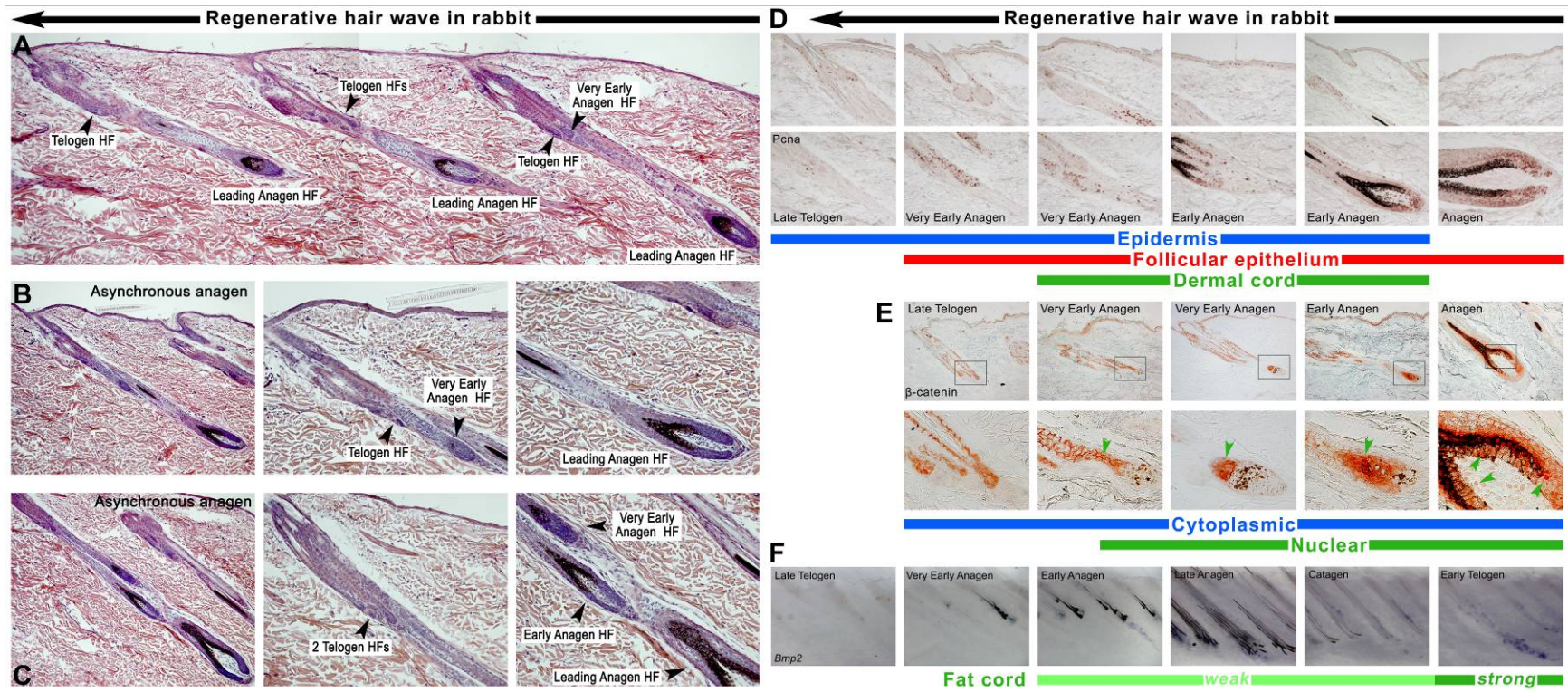
## Microscopic basis of pigmented hair cycle patterns



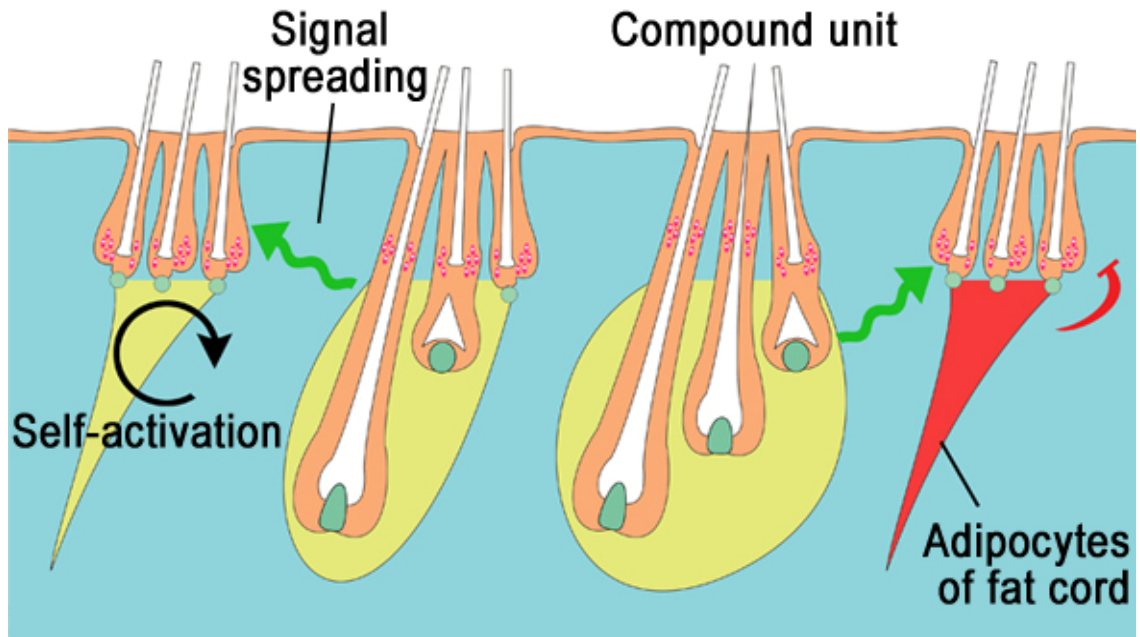
## Initiation modes, Rabbit



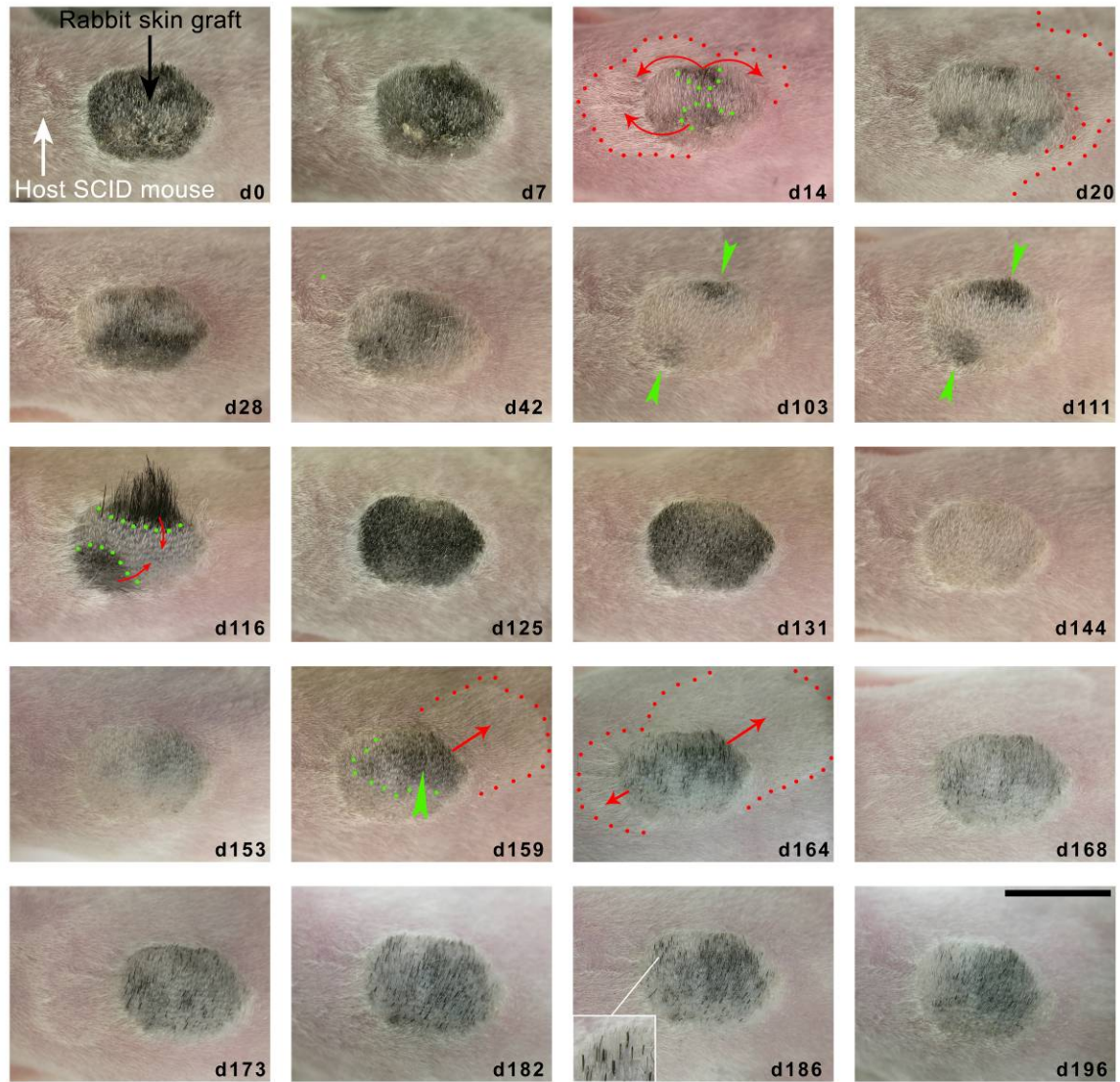
Supplementary Figure 11



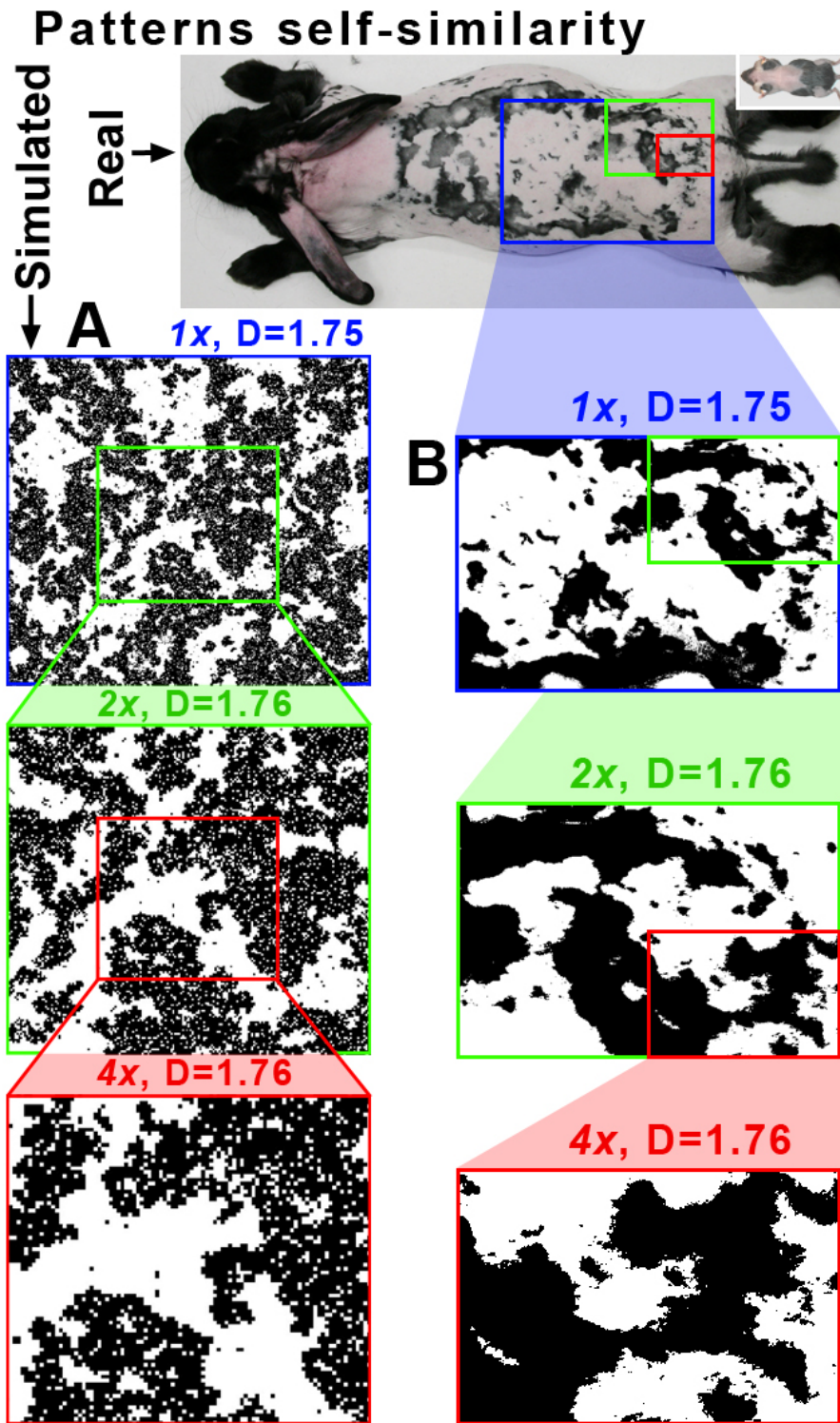
Supplementary Figure 12



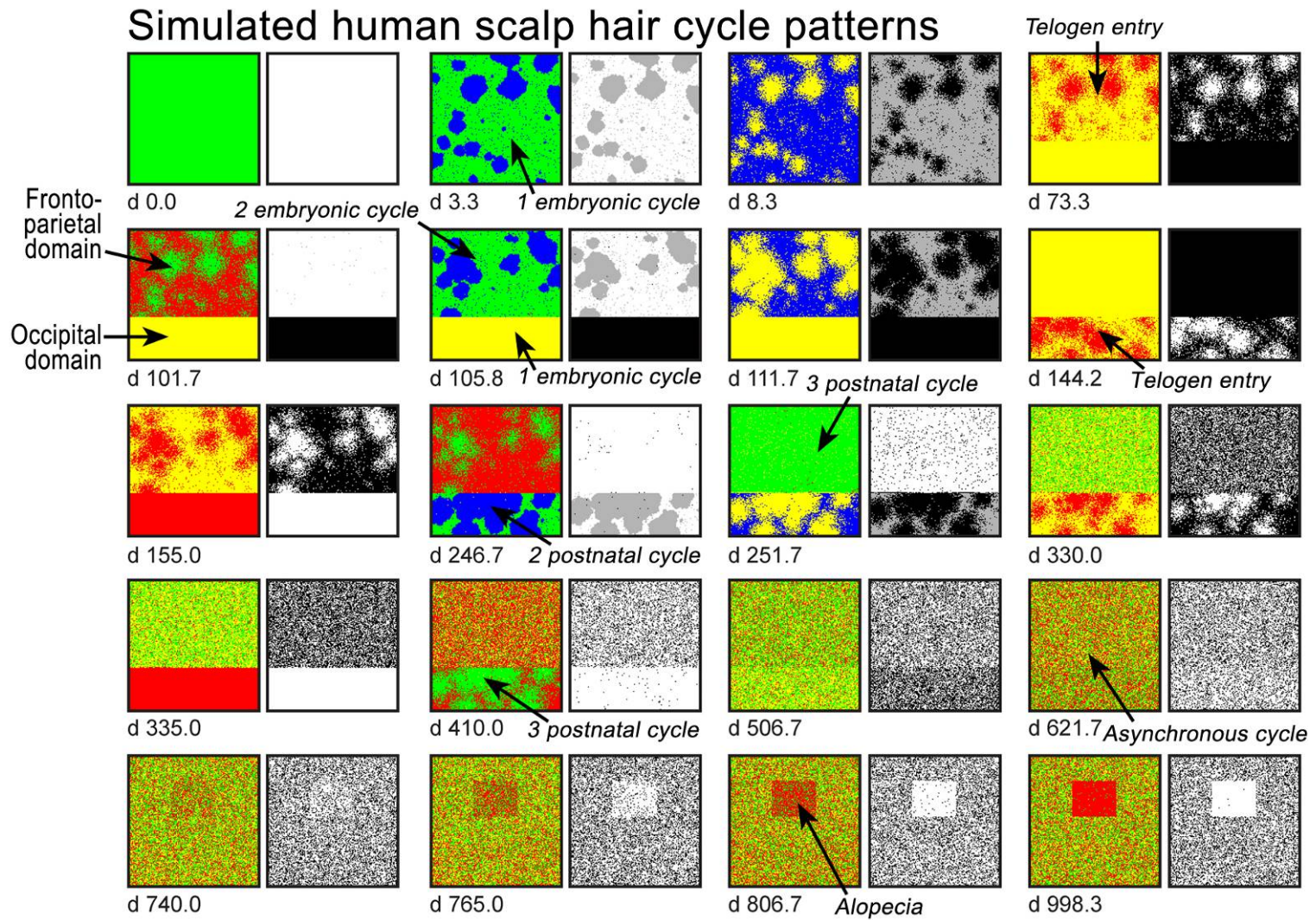
Supplementary Figure 13



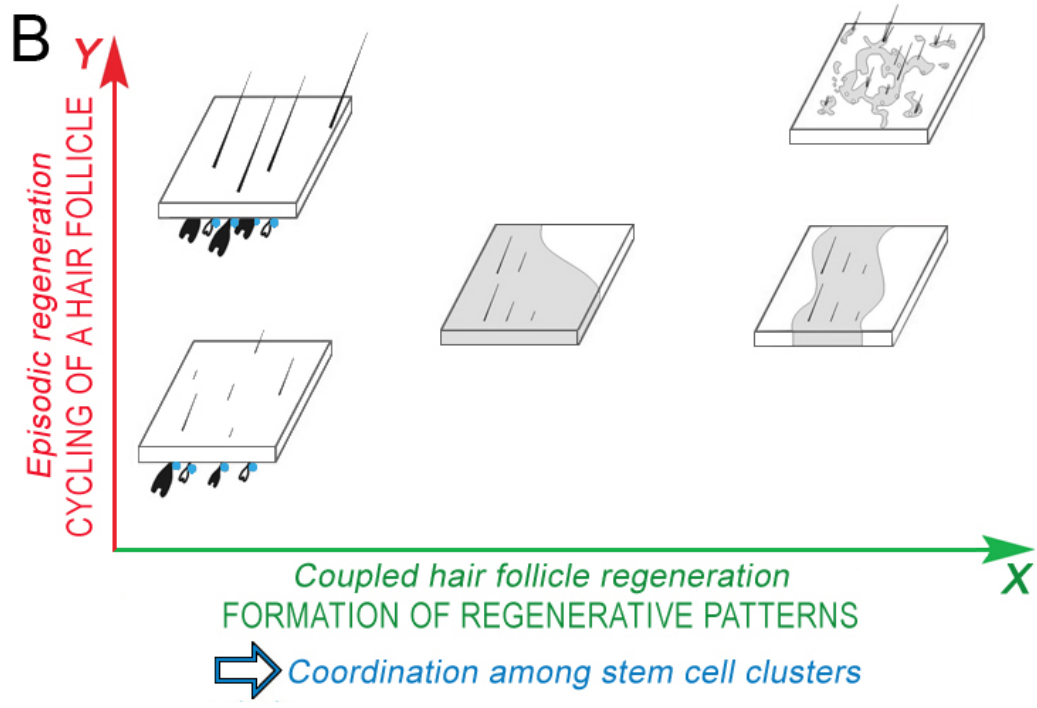
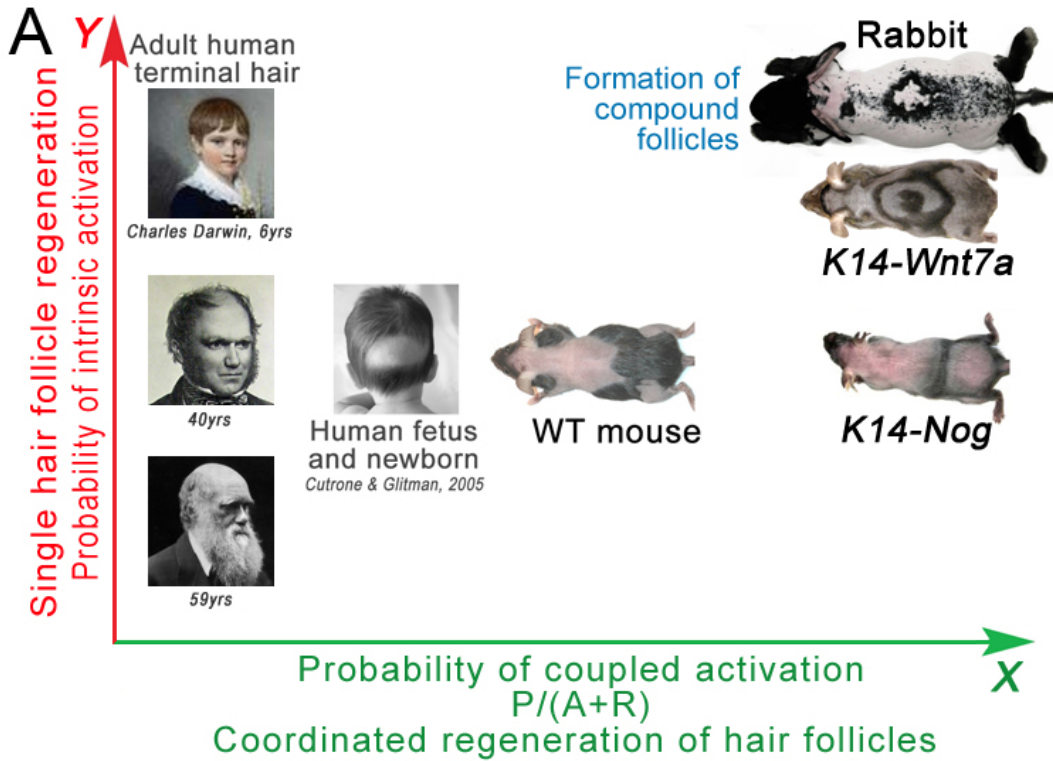
Supplementary Figure 14



Supplementary Figure 15



Supplementary Figure 16



**Supplementary Movies S1-4. Predictive modeling of the regeneration dynamics among hair stem cell clusters with balanced activator/inhibitor levels.** (S1) Spreading of a regenerative wave. (S2) Multiple initiation events. (S3) Borders can be maintained over several cycles. (S4) Border instability. Two types of plots are shown: the right-hand plot shows each automaton state as a different color ( $P$  – blue,  $A$  – yellow,  $R$  – red,  $C$  – green) whilst the left-hand plot shows expected pigmentation states as they would appear on the skin ( $P$  – grey,  $A$  – black,  $R$  and  $C$  – white).

**Supplementary Movies S5-6. Predictive modeling of the regenerative patterns upon progressive increase in activator levels.** The CA model predicts faster global regeneration dynamics when parameters of automaton cycle are adjusted to reflect a progressive rise in activator: (S5, bottom row) duration of  $R$ -phase is shortened; (S6, bottom row) duration of  $R$ -phase is shortened, duration of  $P$ -phase is increased at the expense of  $A$ -phase, minimal number of neighboring automata required to spontaneously enter  $P$ -phase is reduced and probability of spontaneous  $P$ -phase entry is increased. (S5-6, top row) Control simulations performed with balanced activator/inhibitor levels. For each row two types of plots are shown: the right-hand plot shows each automaton state as a different color ( $P$  – blue,  $A$  – yellow,  $R$  – red,  $C$  – green) whilst the left-hand plot shows expected pigmentation states as they would appear on the skin ( $P$  – grey,  $A$  – black,  $R$  and  $C$  – white). See **Supplementary Table 1** for parameter values (S5, bottom row corresponds to “Activators $\uparrow$ ”; S6, bottom row corresponds to “Activators $\uparrow\uparrow$ ”).

**Supplementary Movie S7. Predictive large-scale modeling of the regenerative patterns upon increase in activator levels.** Multiple spontaneous  $C \rightarrow P$  initiation events occur and multiple continuous  $C \rightarrow P$  spreading waves exist simultaneously. As the simulation time increases, complex, fractal-like patterns develop. Two types of plots are shown: the right-hand plot shows each automaton state as a different color ( $P$  – blue,  $A$  – yellow,  $R$  – red,  $C$  – green) whilst the left-hand plot shows expected pigmentation states as they would appear on the skin ( $P$  – grey,  $A$  – black,  $R$  and  $C$  – white). See **Supplementary Table 1** for parameter values.

**Supplementary Movie S8. Predictive modeling of the interaction between fast and slow patterns.** Two types of plots are shown: the right-hand plot shows each automaton state as a different color ( $P$  – blue,  $A$  – yellow,  $R$  – red,  $C$  – green) whilst the left-hand plot shows expected pigmentation states as they would appear on the skin ( $P$  – grey,  $A$  – black,  $R$  and  $C$  – white). Also see fig. S4B.

**Supplementary Movie S9. Model simulations of human scalp hair regenerative patterns.** Modeling performed using a series of assumptions derived from known human scalp hair regenerative behavior during the first and second fetal growth cycles (Cutrone and Grimalt, 2005; Halloy, 2000), as well as during normal adult growth cycles and growth cycles upon alopecia can reproduce human scalp hair regenerative patterns. Two types of plots are shown: the right-hand plot shows each automaton state as a different color ( $P$  – blue,  $A$  – yellow,  $R$  – red,  $C$  – green) whilst the left-hand plot shows expected follicular pigmentation states as they would appear on the skin ( $P$  – grey,  $A$  – black,  $R$

and C – white). Also see fig. **S15** and **Supplementary Table 2**.

**Supplementary Movies 1-9 are available on-line for download from:**

**Movie S1**

[http://www.hairfollicle.com/docs/KGCdR3jhjhe2ss4g4g45ujk5s4w87/movies/Movie\\_S1.mov](http://www.hairfollicle.com/docs/KGCdR3jhjhe2ss4g4g45ujk5s4w87/movies/Movie_S1.mov)

**Movie S2**

[http://www.hairfollicle.com/docs/KGCdR3jhjhe2ss4g4g45ujk5s4w87/movies/Movie\\_S2.mov](http://www.hairfollicle.com/docs/KGCdR3jhjhe2ss4g4g45ujk5s4w87/movies/Movie_S2.mov)

**Movie S3**

[http://www.hairfollicle.com/docs/KGCdR3jhjhe2ss4g4g45ujk5s4w87/movies/Movie\\_S3.mov](http://www.hairfollicle.com/docs/KGCdR3jhjhe2ss4g4g45ujk5s4w87/movies/Movie_S3.mov)

**Movie S4**

[http://www.hairfollicle.com/docs/KGCdR3jhjhe2ss4g4g45ujk5s4w87/movies/Movie\\_S4.mov](http://www.hairfollicle.com/docs/KGCdR3jhjhe2ss4g4g45ujk5s4w87/movies/Movie_S4.mov)

**Movie S5**

[http://www.hairfollicle.com/docs/KGCdR3jhjhe2ss4g4g45ujk5s4w87/movies/Movie\\_S5.mov](http://www.hairfollicle.com/docs/KGCdR3jhjhe2ss4g4g45ujk5s4w87/movies/Movie_S5.mov)

**Movie S6**

[http://www.hairfollicle.com/docs/KGCdR3jhjhe2ss4g4g45ujk5s4w87/movies/Movie\\_S6.mov](http://www.hairfollicle.com/docs/KGCdR3jhjhe2ss4g4g45ujk5s4w87/movies/Movie_S6.mov)

**Movie S7**

[http://www.hairfollicle.com/docs/KGCdR3jhjhe2ss4g4g45ujk5s4w87/movies/Movie\\_S7.mov](http://www.hairfollicle.com/docs/KGCdR3jhjhe2ss4g4g45ujk5s4w87/movies/Movie_S7.mov)

**Movie S8**

[http://www.hairfollicle.com/docs/KGCdR3jhjhe2ss4g4g45ujk5s4w87/movies/Movie\\_S8.mov](http://www.hairfollicle.com/docs/KGCdR3jhjhe2ss4g4g45ujk5s4w87/movies/Movie_S8.mov)

**Movie S9**

[http://www.hairfollicle.com/docs/KGCdR3jhjhe2ss4g4g45ujk5s4w87/movies/Movie\\_S9.mov](http://www.hairfollicle.com/docs/KGCdR3jhjhe2ss4g4g45ujk5s4w87/movies/Movie_S9.mov)